

Potential of double pilot injection strategies optimized with the design of experiments procedure to improve diesel engine emissions and performance

*Original*

Potential of double pilot injection strategies optimized with the design of experiments procedure to improve diesel engine emissions and performance / D'Ambrosio, Stefano; Ferrari, Alessandro. - In: APPLIED ENERGY. - ISSN 0306-2619. - 155:(2015), pp. 918-932. [10.1016/j.apenergy.2015.06.050]

*Availability:*

This version is available at: 11583/2628093 since: 2016-01-13T17:18:20Z

*Publisher:*

Elsevier Ltd

*Published*

DOI:10.1016/j.apenergy.2015.06.050

*Terms of use:*

This article is made available under terms and conditions as specified in the corresponding bibliographic description in the repository

*Publisher copyright*

Elsevier postprint/Author's Accepted Manuscript

© 2015. This manuscript version is made available under the CC-BY-NC-ND 4.0 license  
<http://creativecommons.org/licenses/by-nc-nd/4.0/>. The final authenticated version is available online at:  
<http://dx.doi.org/10.1016/j.apenergy.2015.06.050>

(Article begins on next page)

1 **POTENTIAL OF DOUBLE PILOT INJECTION STRATEGIES OPTIMIZED WITH A**  
2 **DESIGN OF EXPERIMENTS PROCEDURE TO IMPROVE DIESEL ENGINE**  
3 **EMISSIONS AND PERFORMANCE.**

4 *d'Ambrosio, S. , and Ferrari, A.\**

5 *Energy Department – Politecnico di Torino*

6 *C.so duca degli Abruzzi, 24, 10129, Torino, Italy.*

7 **ABSTRACT**

8 The potential of pilot-pilot-main triple injection strategies versus engine out emissions, combustion noise and brake  
9 specific fuel consumption has been assessed experimentally on a Euro 5 diesel engine with a reduced compression ratio  
10 (16.3:1). The engine has been fueled with conventional diesel fuel. The experimental tests on the engine have been  
11 carried out in a dynamometer cell under different steady state working conditions, that are representative of passenger  
12 car engine applications over the European homologation cycle. Furthermore, in-cylinder analyses of the pressure, heat-  
13 release rate, temperature and emissions have been performed in order to obtain more detailed knowledge on the cause-  
14 and-effect-relationships between the implemented injection strategies and the results of the experimental tests.

15 The implemented double-pilot injection engine calibrations have been optimized by means of the design of experiments  
16 procedure. The plotted data of the engine performance and emissions have been compared with data from the original  
17 double-injection schedule, characterized by a retarded main injection timing, in order to intensify the premixed  
18 combustion phase. The benefits and the disadvantages of the *PCCI* concept are preliminarily discussed, on the basis of  
19 the experimental pilot-main injection strategy results.

20 The substitution of the pilot-main injection schedule with the triple injection, for light engine loads and low engine  
21 speeds, has led to higher combustion pressures, lower heat release rates, shorter ignition delays and lower brake specific  
22 fuel consumption. Above all, a significant improvement in engine noise and in both *CO* and *HC* engine-out emissions  
23 has been achieved and the *NO<sub>x</sub>* emission have been limited by the application of high *EGR* rates. When medium engine  
24 loads and speeds are analyzed, the considered double-pilot injection strategy allows the *NO<sub>x</sub>* emissions to be reduced,  
25 compared to the baseline pilot-main injection schedule. However, the combustion noise does not improve and the soot  
26 deteriorates, even though the soot penalties are not relevant.

---

\* Corresponding author e-mail address: [alessandro.ferrari@polito.it](mailto:alessandro.ferrari@polito.it).

27 **Keywords:** pilot injections; design of experiments; partial premixed charge compression ignition engines.

## 28 **Highlights:**

- 29 - The benefits and the weak points of the partial *PCCI* strategy for low loads and speeds are discussed.
- 30 - The effects of the triple pilot-pilot-main injection on engine-out emissions and noise are analyzed.
- 31 - The experimental tests on the multiple injections are supported by numerical in-cylinder analyses.

## 32 **1. INTRODUCTION**

33 The implementation of a pilot injection in diesel engines makes the entire amount of the fuel chemical energy be  
34 released over a prolonged time interval, thus determining a longer combustion than for the single injection case.  
35 Furthermore, the premixed combustion of some of the pilot injected fuel causes a slight increase in the in-cylinder gas  
36 pressure and temperature [1] before the main injection has occurred, and therefore leads to a considerable reduction in  
37 the ignition delay of the main injection [2]. This reduction in the fuel ignition delay limits the impact of the premixed  
38 combustion and generates a less rapid heat release rate [3] during the main injection than in a single injection schedule  
39 [4]. As a consequence, the main combustion becomes predominantly mixing-controlled [3].

40 A pilot injection that is sufficiently close to the main injection has the potential of enhancing combustion efficiency and  
41 thus brake specific fuel consumption (*bsfc*), because the pilot and main combustions are linked smoothly [5]. Pilot  
42 injections are also effective in decreasing combustion noise (*CN*), especially at engine idle [3]. Reductions of up to 5-8  
43 dB are generally obtained in the *CN*, compared to single injection strategies [6-8].

44 Since the pilot injection decreases the impact of the overall premixed combustion, it makes the highest flame  
45 temperatures diminish and, as a consequence, the  $NO_x$  emissions generally also reduce, compared to the single-injection  
46 strategy [9]. However, large pilot injected quantities make the  $NO_x$  produced in the pilot combustion grow, and the  
47 increase in the  $NO_x$  amount produced by the pilot combustion can surpass the decrease in the main combustion  $NO_x$   
48 emissions, due to the shortened ignition delay [10]. Furthermore, when heavy *EGR* rates (~60%) are employed, such as  
49 in partial *PCCI* strategies, the pilot injection timing and mass do not influence the  $NO_x$  emissions to any appreciable  
50 extent because the  $NO_x$  emissions are very small [5].

51 The smoke emission in pilot-main injections generally tends to increase, compared to single injections: In fact, the pilot  
52 injection increases the in-cylinder temperature and decreases the oxygen concentration in the gases before the main  
53 injection has occurred. Both of these effects generally make the smoke emission grow: the increased temperature  
54 mainly acts by reducing the lift-off length, which pertains to the main injection, with a subsequent increase in the  
55 equivalence ratios close to the nozzle. The insufficient mixing of fuel with air, which is also due to the shortened

56 ignition delay of the main injection, augments the percentage of the diffusion combustion in the main combustion and,  
57 as a consequence, the final soot level grows [11]. In general, the quantity of the pilot injection should be below a certain  
58 threshold (a general value of 4 mg is normal) in order to contain the smoke number [12].

59 Finally, *HC* and *CO* emissions reduce at low loads if a pilot injection is implemented, because the occurrence of  
60 overmixing is ~~more~~ less likely. In particular, the *CO* conversion rate improves because of the relatively high in-cylinder  
61 temperature and the shorter ignition delay of the fuel injected in the main injection [4].

62 The pilot injection can be exploited in different ways to improve engine-out emissions, *CN* and fuel consumption,  
63 depending on the working condition [13]. Soot emissions are not relevant at low engine speeds and loads, *NO<sub>x</sub>* and  
64 noise are usually controlled, at these conditions, by means of adequate *EGR* rates. The pilot injection is generally  
65 optimized, on the basis of the *EGR* rate, in order to reduce *HC* and *CO* emissions [14], which tend to be high, due to the  
66 presence of lean and cool regions. The *HC* and *CO* emission situation becomes worse at engine cold start and warm-up,  
67 when the oxidation catalyst has less conversion efficiency. Soot, *NO<sub>x</sub>*, noise and *bsfc* are the dominant problems at  
68 medium load conditions, that is, in the higher load zone of the *NEDC* region, whereas *HC* and *CO* are not of great  
69 concern. Pilot injections are therefore used in these conditions to improve *PM-NO<sub>x</sub>* and *bsfc-NO<sub>x</sub>* trade-offs and, above  
70 all, *CN* [15].

71 Pilot injection is generally applied to the *NEDC* area, but it can also be used for other purposes and offers other benefits.  
72 An early pilot injection can be applied to increase the in-cylinder pressure at the end of the compression stroke during  
73 engine cranking, thus reducing the engine start time. Furthermore, pilot-main injection patterns reduce the cycle-to-  
74 cycle variability of the torque, compared to single injections [4], and this induces more stable engine operation,  
75 especially after the engine crank phase [16]. Finally, pilot injection can be used at full load to limit the peak in-cylinder  
76 pressure and the engine exhaust temperature. The noise due to combustion is less important at these engine working  
77 conditions, since other sources of noise dominate in the vehicle, and the pilot injection therefore allows either the fuel  
78 rate to be increased or the mechanical and thermal stresses in the engine to be reduced, thus providing possible weight  
79 savings or simplifications of the cooling circuit. Instead, when the maximum torque is smoke limited, an early pilot  
80 injection can increase the full load torque by improving the utilization of the air within the cylinder, compared to the  
81 case of a single injection with a long energizing time [17]. In general, the pilot injection shot can also be used at high  
82 loads to reduce soot and improve combustion efficiency, since the main injection duration can be shortened.

83 The fundamental pilot-main injection scheme constitutes the conceptual basis for the development of more  
84 sophisticated and advanced multiple injection strategies that can implement multiple pilot injection shots. Pilot-pilot-  
85 main injection schedules have been shown to have a great potential toward noise [18, 19], emission [20, 21] and *bsfc*  
86 [20, 22, 19] reductions. However, more trials are required to optimize various engine parameters, such as the *EGR* rate,

the swirl actuator position, the boost pressure, the dwell-time, the injection timings, the rail pressure and the energizing times of all of the injection shots, and thus to be able to fully exploit these strategies [23]. In the present work, a design of experiment (*DoE*) procedure has been applied to optimize the double-pilot injection engine calibration. This innovative approach allows the effective benefits of this injection strategy to be assessed, since optimized pilot-pilot-main and pilot-main injection engine calibrations are compared. In general, the aims of the double-pilot injection strategy should be selected on the basis of the engine working conditions and the installed aftertreatment devices. The triple injection in the current investigation is principally aimed at minimizing  $NO_x$  and combustion noise. Furthermore, the double- and triple-injection strategies are tested under high *EGR* conditions, whereas most of the research on multiple injections has been conducted under low or moderate *EGR* rates (moderate *EGR* rates correspond to *EGR* fractions up to 30-40%) [24].

## 2. EXPERIMENTAL FACILITIES AND ENGINE SETUP.

The experimental tests have been carried out on the dynamic test bed installed at the Politecnico di Torino *IC* laboratories. The test rig is equipped with an ‘*ELIN AVL APA 100*’ cradle-mounted *AC* dynamometer, featuring nominal torque and power of 525 Nm and 220 kW, respectively, as well as a maximum speed of 12000 rpm. The facility is capable of full four-quadrant operation with high speed and torque dynamics, as well as the simulation of zero torque and gear shifting oscillations in the drivetrain.

The test facility is equipped with a ‘*Pierburg AVL AMA 4000*’ raw exhaust-gas analyzer, which is basically made up of three analyzer trains. Two of these trains feature the following modules: one heated flame ionization detector for the *THC* analysis, one heated chemiluminescence detector for the analysis of the  $NO_x$ , three nondispersive infrared analyzers for the measuring of low as well as high *CO* and  $CO_2$  concentration levels and one paramagnetic oxygen detector for the  $O_2$  levels. These two trains allow the pollutant emissions to be measured simultaneously, upstream and downstream of the aftertreatment system. The third train is made up of a  $CO_2$  concentration detector for the measuring of the  $CO_2$  concentrations in the inlet manifold, in order to be able to calculate the *EGR* mass fraction, which is defined as  $X_{EGR} = \dot{m}_{EGR} / (\dot{m}_{EGR} + \dot{m}_a)$ , according to the procedure developed in [25].

As far as the particulate matter (*PM*) measurement is concerned, the dynamic test bed is equipped with the following instruments: *AVL 415S* smokemeter, *AVL 439S* opacimeter and *AVL SPC472* Smart Sampler. Finally, an ‘*AVL KMA 4000* Methanol’ measuring system continuously meters the engine fuel consumption. This system is based on the *AVL PLU* measuring principle of a servo-controlled positive displacement counter, and it can perform measurements over the 0.28-110 kg/h range with a reading accuracy of 0.1% for diesel fuel.

116 All of the abovementioned measurement devices are controlled by a *PUMA OPEN 1.3.2* automation system, which also  
117 includes *ISAC 400* software for the simulation of the behavior of both the vehicle (road load, road gradient and  
118 moments of inertia of the driveline components, which are not physically present on the test bed) and of the driver  
119 behavior (use of the clutch, accelerator pedal and gear shifting).

120 The tested engine, the main features of which are reported in Table 1, is a Euro 5 engine fueled with conventional diesel  
121 oil. It has been fully instrumented with piezoresistive pressure transducers and thermocouples for the measurement of  
122 the pressure and temperature levels at the following locations: upstream and downstream of the compressor, at the inlet  
123 manifold, upstream and downstream of the turbine and downstream of the aftertreatment system. Additional  
124 thermocouples have also been installed for the measurement of the temperatures downstream of the intercooler, in the  
125 four inlet and exhaust runners, as well as upstream and downstream of the *EGR* cooler. Finally, an *UEGO* air-fuel ratio  
126 sensor has been located within the exhaust system. The acquisition of all of these time-averaged quantities are directly  
127 managed directly by the *PUMA OPEN 1.3.2* system, through a dedicated firewire front-end module, which can manage  
128 up to 48 analog input channels with a maximum data capture rate of 5 kHz per channel.

129 A high-frequency piezoelectric transducer has been installed on the engine cylinder head to measure the pressure time-  
130 history of the gases in one of the cylinders, whereas another high-frequency piezoresistive transducer has been used to  
131 detect the pressure levels in the inlet runner of the same cylinder in order to reference the in-cylinder pressure. An *AVL*  
132 *365C* crank-shaft driven encoder generates the time base for an automatic 14 bit data-acquisition system (based on the  
133 *AVL* indimodul 620 system), which is capable of acquiring up to 8 channel data with a maximum frequency of 800 kHz  
134 per channel. The acquisition system is managed by *AVL Indicom* software, in order to allow both the online analysis of  
135 the indicated cycle and data storage operation for post-processing with a validated three-zone combustion diagnostic  
136 tool [26]. In this model, the combustion chamber content is divided into three zones: a fuel zone, an unburned gas zone,  
137 (containing fresh-air, residual gas and *EGR*) and a burned gas zone obtained from a global stoichiometric combustion  
138 process. Ordinary differential mass and energy conservation equations are applied to the three zones and are solved  
139 numerically on the basis of the experimental in-cylinder pressure. The model allows the temperatures of the three zones  
140 to be predicted as functions of the crank angle. Furthermore, thermal and prompt NO mechanisms are implemented in  
141 the code, according to the Zeldovich and Fenimore submodels, respectively. The soot formation is modeled [27] by  
142 means of an expression that uses the mean air-fuel ratio over the combustion interval, whereas the soot oxidation rate is  
143 modeled using an empirical formula, based on the temperature of the burned gas zone.

### 144 3. THE DESIGN OF THE EXPERIMENT PROCEDURE

145 The tested engine was calibrated by the *OEM* with a double injection strategy, which represented the state-of-the-art  
146 pilot-main injection schedule for the considered engine technology.

147 The *ppM* injection strategies have been optimized by adopting the statistical design of the experiments (*DoE*) technique.  
148 The following parameters were considered as the most relevant input variables for the procedure: rail pressure ( $p_{Rail}$ ),  
149 swirl actuator position ( $S_w$ ), dwell times ( $DT$ ) between consecutive injections ( $DT_2$  between the pilot 2 and pilot 1 shots  
150 and  $DT_1$  between the pilot 1 and main shots, where pilot 1 is the closest shot to the main injection and pilot 2 the  
151 furthest shot from the main injection), main injection timing ( $SOI_{Main}$ ), the injection quantities in each shot ( $q_{Pil1}$  and  
152  $q_{Pil2}$ ) and the inducted air per stroke and per cylinder ( $m_a$ ).

153 Key-points are engine working points (characterized in terms of  $b_{mep}$  [bar] and speed  $n$  [rpm]), considered as  
154 representative of the engine application to a passenger car over the new European driving cycle. The following key-  
155 points were considered for the tested engine ( $n \times b_{mep}$ ):  $1500 \times 2$ ,  $1500 \times 5$ ,  $2000 \times 2$ ,  $2000 \times 5$ ,  $2500 \times 8$ ,  $2750 \times 12$  and idle.

156 Tables 2 and 3 report (second column) the parameter levels that were considered in the variation lists for the  
157 optimization of the *ppM* injection schedule at the  $1500 \times 2$  and  $2000 \times 5$  key-points. The center and the extreme values of  
158 the range that were considered for each parameter were chosen on the basis of preliminary measurements. An  
159 appropriate number of levels was selected in order to obtain accurate results with a reasonable number of tests for each  
160 variation list. The quantity of fuel in the main injection is set by the test-bench control system in order to guarantee the  
161  $b_{mep}$  value, and is therefore not present as a parameter in the variation list. The *EGR* ratio affects the emissions at the  
162 diesel engine exhaust to a great extent. However, the *ECU* does not evaluate this parameter directly, but can measure  $m_a$   
163 (by means of the air mass flowmeter), which is intimately connected to *EGR*. Therefore, the information related to the  
164 induced air,  $m_a$ , was considered in the variation lists, instead of the *EGR* ratio.

165 The preliminary variation list was obtained using the Matlab Model-Based Calibration toolbox, setting a V-optimal type  
166 design of experiments, which minimizes the prediction error variance, and a full factorial series, as the candidate set, on  
167 the basis of the levels shown in Tables 2 and 3. The preliminary variation list was then randomized and replications of  
168 the central point (defined by the center value of each parameter range) were added every 10-15 points in order to further  
169 reduce the prediction error variance and check for any possible drifts of the output variables for fixed input parameters.  
170 The final variation lists were made up of 120-150 tests for each considered key-point. Once the variation list tests had  
171 been carried, it was possible to obtain quadratic models of the output variables as functions of the input variables and of  
172 their interactions.

173 The engine-out specific  $NO_x$ ,  $CO$ ,  $HC$  and soot emissions, the  $bsfc$  and the  $CN$  were considered as the output variables.

174 Different targets can be introduced for the output variables in order to select the best set of values for the input variables

at each key point, that is, the optimized engine calibration. The optimization procedure consists of a number of constraints on the output variables. These constraints depend on the pollutant emission regulations, on the aftertreatment devices that are installed on the engine, on the  $CO_2$  targets and on aspects related to fun to-drive.

The considered Euro 5 engine was equipped with a diesel oxygen catalyst (*DOC*) and a particulate filter, but no aftertreatment device was designed to reduce the  $NO_x$  emissions. The optimization strategy for the triple (pilot-pilot-main) injection schedules, based on the *DoE*, was aimed at minimizing  $NO_x$  emissions and at reducing the combustion noise with respect to the pilot-main injection calibration, which was originally implemented in the ECU provided by the engine *OEM*. However, rather severe upper limits were also set for  $CO$ ,  $HC$  and *bsfc*.

Tables 4 and 5 show the reference values of the output variables for the pilot-main injection strategy and the constraints used for the optimization of the triple injection strategy. The optimum values of the input variables, calculated by means of the *DoE* procedure, are reported in the third column of Tables 2 and 3. *EGR* trade-offs were performed in the neighborhood of the calibration baseline points for both the double and the optimized triple injection strategies in order to compare not only the baseline points of the two calibrations, but also two complete curves.

## 4. LIGHT LOAD CONDITIONS.

### 4.1 PCCI-like double-injection strategies

Figures 1-3 report the in-cylinder pressure ( $p_{cyl}$ ), the heat release rate (*HRR*) and the burned gas temperature ( $T_b$ ) time histories, respectively, for  $n = 1500$  rpm and  $bmeP=2$  bar. The continuous curves with square- and circle-symbols refer to  $X_{EGR}\approx 50\%$  and  $X_{EGR}\approx 28\%$ , respectively (these two operating conditions correspond to high and moderate *EGR* rates), and the same pilot-main (*pM*) strategy is adopted in both cases. Since the injection strategy is the same, these preliminary tests are aimed at assessing the effect of the *EGR* rate in *PCCI* engines. The  $p_{cyl}$  trace has been measured by means of the piezoresistive pressure transducer installed in the combustion chamber, while the *HRR*, and the  $T_b$  time histories have been calculated by means of the three-zone combustion diagnostic tool.

A relatively high dwell time between the pilot and the main injection ( $DT\approx 1400\ \mu s$ ) has been implemented (cf. Fig. 2) and a vigorous swirl has been applied to promote the air-to-fuel mixing. The heavy *EGR* rate condition that corresponds to  $X_{EGR} \approx 50\%$  has been applied in order to prolong the fuel ignition delay and obtain a partially homogeneous mixture before ignition [28]. Fig.1 shows that the in-cylinder pressure decreases as the *EGR* is increased. In fact, both the flow-rate through the turbine and the upstream pressure are reduced when high *EGR* rates are applied to a short-route *EGR* system (cf. also the schematic of the engine in Table 1). As a consequence, the system may not be able to maintain the desired boost level and a decrease in the boost may therefore be experienced at high *EGR* rates, especially for low



204 loads. The decrease in the in-cylinder pressure with increasing  $EGR$  in Fig. 1 is due to the reduction in the boost  
 205 pressure and to the increase in the temperature of the cooled  $EGR$ , compared to the temperature of the fresh air coming  
 206 from the engine intercooler. Figs. 2 and 3 show that high fractions of cooled  $EGR$  and retarded main injection timings  
 207 allow the maximum  $HRR$  and the  $T_b$  peak value to be contained [29], and the ignition delay of both the pilot and main  
 208 injected fuel to be lengthened, compared to the moderate  $EGR$  rate condition ( $X_{EGR} \approx 28\%$ ). In particular, it can be  
 209 observed that the pilot combustion in the  $X_{EGR} \approx 50\%$  case exhibits a two-stage ignition with the presence of both cool  
 210 and hot flame reactions, whereas single-stage pilot combustion occurs at  $X_{EGR} \approx 28\%$ .  
 211 The considered pilot-main ( $pM$ ) injection schedule realizes a highly premixed combustion concept, since the main  
 212 combustion event starts when the main injection has finished. Most of the fuel injected during the pilot and the main  
 213 shots burns in premixed combustion conditions. The  $HRR$  peak, related to the diffusive combustion of the main injected  
 214 fuel, can be seen in Fig. 2 for  $X_{EGR} \approx 28\%$ , but vanishes for  $X_{EGR} \approx 50\%$ . The advantage of the implemented strategy is that  
 215 it induces a simultaneous reduction in soot and  $NO_x$  emissions, due to the intensified fuel premixing and to the reduced  
 216 combustion temperature. Fig. 4 shows that both the soot and  $NO_x$  emissions decrease when the  $EGR$  rate is increased  
 217 progressively, while the other engine parameters remain constant (the contoured triangle symbol represents the  $EGR$   
 218 rate of the baseline pilot-main injection calibration); this behavior, with respect to  $X_{EGR}$ , is not observed when more  
 219 conventional double-injection patterns are applied. Fig. 5 shows the gas temperature at the diesel oxygen catalytic  
 220 catalyst inlet ( $T_{cat}$ ) as a function of the  $EGR$  rate. The experimental points, evaluated as functions of  $NO_x$  in Fig 4 and as  
 221 functions of  $EGR$  rate in Fig.5, are the same (maximum  $NO_x$  corresponds to minimum  $X_{EGR}$  and vice versa).  
 222 Higher  $X_{EGR}$  levels than 50% are in line with partial  $PCCI$  applications, which intensify the local mixing of the fuel  
 223 plume and the charge, with the production of a premixed stratified charge. Furthermore, the selected engine  
 224 compression ratio was  $\varepsilon = 16.3$ , which falls between the typical values of conventional diesel engines ( $\varepsilon = 17 \div 18$ ) and the  
 225 characteristic values of partial  $PCCI$  engines ( $\varepsilon = 13 \div 16$ , [30]). The reduced compression ratio makes the temperature  
 226 and pressure, which are closely related to  $NO_x$  formation, decrease during the compression phase. This enables the fuel  
 227 spray to penetrate further with more air entrainment, thus contributing to a decrease in the soot [31], which is also due  
 228 to the increase in the fuel autoignition delay [32, 33]. Finally, a toroidal combustion-bowl was selected, in line with  
 229 partial  $PCCI$  applications, since it assures a rapid fuel mixing when combined with a high swirl number, and a large  
 230 bowl piston diameter was designed in order to reduce the occurrence of wall impingement. However, unlike typical  
 231 partial  $PCCI$  combustion diagrams, the pilot injected fuel does not burn together with the main injected fuel, and a pilot  
 232 combustion event, which is not connected to the main combustion, can be observed in the  $HRR$  traces reported in Fig. 2.  
 233 Furthermore, the ratio of the quantity injected in the main shot to that injected in the pilot shot is significantly higher  
 234 than that usually adopted in partial  $PCCI$  engines.

Pilot injection quantities with early injection timings, like the typical ones used in early *PCCI* injection strategies (40-50 *BTDC* degrees), can cause the fuel vapor to spread to the cylinder liner, because the in-cylinder charge pressure and density are low for early injection timings and light loads. This leads to overmixed regions and wall quenching phenomena, both of which are important sources of *HC* and *CO* emissions. In addition, the possible spray impingement on the wall surfaces dramatically increases the amount of unburned hydrocarbons [34], dilutes the lubrication oil and causes the fuel consumption to increase to a great extent, since part of the pilot injected fuel is wasted and unable to ignite. For these reasons, the relatively long dwell time in the pilot-main injection pattern, which is reported in Fig. 2, has been introduced by further delaying the main injection rather than by advancing the pilot injection. Since the pilot injection does not occur very early during the piston compression stroke, and the pilot injected quantity is contained ( $V_{pi} \approx 1.7 \text{ mm}^3$ ), wall impingement occurrence is not a concern. Furthermore, the retarded main combustion contributes to the generation of a reduced soot formation rate because the peak in-cylinder temperature around *TDC* is contained and an enhanced soot oxidation rate can be observed during expansion and blowdown phases, due to the raised burned gas temperatures during the last part of the expansion stroke and at the engine exhaust.

The considered *pM* injection pattern features high levels of *HC* and *CO* emissions, due to low-temperature combustion [35] and fuel overmixing, as well as elevated combustion noise, due to the highly premixed combustion. Furthermore, the *bsfc* become worse, compared to the double injection strategies implemented in conventional diesel engines, due to the retarded main injection timing ( $SOI_{Main}$ ) and the diminished  $\varepsilon$  value. These drawbacks are of the same typology as those encountered in classic partial *PCCI* engines featuring late injection strategies.

A minimum temperature level of 200°C is necessary at the catalytic converter inlet ( $T_{cat}$ ) to obtain a satisfactory efficiency of the diesel oxygen catalyst (*DOC*) for the conversion of the high *HC* and *CO* engine-out emissions at low loads. The  $T_{cat}$  values in Fig. 5 can be seen to be higher than this threshold for  $X_{EGR} > 45\%$ .

Since the main injected quantity is much larger than the pilot injected mass, the  $SOI_{Main}$ , which is equal to 1° *CA ADTC* in Fig. 2, has not been delayed any further, as occurs in typical late *PCCI* injection strategies, in order to avoid an excessive *bsfc* penalty. In fact, the  $SOI_{Main}$  varies within the 3-10° *CA ATDC* range for late *PCCI* injection strategies, whereas it is usually in the 5-7° *CA BTDC* range for diesel engines with conventional combustion systems.

## 4.2 Triple injection strategies.

Figures 6-8 show comparisons of *HC-NO<sub>x</sub>*, *CO-NO<sub>x</sub>* and *bsfc-NO<sub>x</sub>* *EGR* trade-off curves obtained for two different engine calibrations in the 45% <  $X_{EGR}$  < 55% range and at  $n = 1500 \text{ rpm}$  and  $bme_p = 2 \text{ bar}$ . Fig. 9 instead plots the *NO<sub>x</sub>*- $X_{EGR}$  curves for the two strategies. The triangle symbols in Figs. 6-9 pertain to the previously discussed *pM* injection engine calibration, whereas the circle symbols refer to a pilot-pilot-main (*ppM*) injection engine calibration. The

contoured line symbols correspond to the baseline calibration points of the two strategies. The triple injection baseline calibration has been obtained with the *DoE* campaign; not only has a pilot shot been added to the injection train of the baseline point of the *pM* calibration, but the rail pressure, injection timings, energizing times and other engine parameters have also been changed. The *SOI* of the pilot 1 and pilot 2 injections are in the 10÷20 cad *BTDC* range for the *ppM* strategy, and are in line with the literature results concerning the best pilot injection timings in triple injections [4].

It can be observed, from Figs. 6-9, that the *DoE* optimized *ppM* strategy generally allows the *CO* and *HC* emissions to be improved at the same *NO<sub>x</sub>*, with respect to the baseline double injection strategy. Furthermore, a slight enhancement can be detected for the *bsfc-NO<sub>x</sub>* trade-off. If reference is made to the calibration baseline points, the *NO<sub>x</sub>* engine-out emissions reduce in the *ppM* case (Fig. 9), in line with [36]. However, the *NO<sub>x</sub>-X<sub>EGR</sub>* curve is virtually the same for the two strategies and the effectiveness of the *EGR* on the engine-out *NO<sub>x</sub>* emissions therefore does not change for either of the two calibrations.

The *ppM* pattern should lead to a decrease in the local air-to-fuel ratio, with respect to time and space, due to the lower global oxygen concentration ( $[O_2]_{int}=14.9$  versus  $[O_2]_{int}=16.0$  of the *pM* calibration). The generation of a suitable fuel vapor stratification close to the nozzle reduces the impact of fuel overmixing and wall quenching, and thus decreases the engine out *HC* and *CO* emissions (cf. Figs. 6 and 7). In other words, the pre-combustion, which is due to the introduction of the pilot 1 injection prior to the main injection, plays a role in attaining a sufficient main combustion ignition and in improving the conversion efficiency of the fuel, and thus in enhancing the complete combustion of the main injection. The improvements obtained for the *bsfc*-, *HC*- and *CO-NO<sub>x</sub>* tradeoffs, by means of the pilot-pilot-main injection, are in line with the results found in [19-22] for low loads and speeds. In particular, when *EGR* rates close to 50% are applied, two pilot injections are recommended [15] in order to decrease the *HC* emissions.

The *p<sub>cyl</sub>* and the *HRR* curves that refer to the calibration baseline points of both the *pM* and the *ppM* strategies are reported in Figs. 10 and 11, respectively. The *pM* curves have been plotted with solid line and triangle symbols, whereas the *ppM* solid line curves are marked with circle symbols. The two-stage autoignition delay of the pilot 2 injection increases for the *ppM* strategy because the pilot 2 injection takes place earlier in the compression stroke, where the charge pressure and temperature are lower. Furthermore, the maximum *p<sub>cyl</sub>* value pertaining to the main injection increases when passing from the *pM* to the *ppM* injection schedule, but the *HRR* pilot peaks and the *HRR* main combustion peak reduce when pilot 1 injection is applied because of the decrease in the premixed combustion portion. This evidence on *p<sub>cyl</sub>* and *HRR* proves that the combustion performance has improved, and the *p<sub>cyl</sub>* and *HRR* trends with the number of injections can be confirmed from those obtained passing from a single injection to one-pilot injection. As can be seen in Fig. 12, the decrease in the maximum *HRR* and the earlier main combustion induce a slight diminution in

296 temperature  $T_b$  of the burned gases for  $\theta \geq 370^\circ CA$  in the case of the *ppM* strategy. On the other hand, the earlier  $SOI_{pil2}$   
 297 of the *ppM* strategy advances the time instant at which the burned gas temperature jumps to high levels and, as a  
 298 consequence, the residence time in which the burned gases are exposed to higher temperatures than 1900 K increases  
 299 for the triple injection calibration. The  $NO_x$  formation rates are very sensitive to flame temperatures above 1900-2000 K  
 300 [37], but, on the basis of the Kamimoto-Bae diagram,  $NO_x$  emissions are only produced for smaller local equivalence  
 301 ratios ( $\phi$ ) than 1.5 [38]. A larger amount of mixture with relatively high  $\phi$  values should be obtained in the fuel spray for  
 302 the *ppM* strategy, because of the reduced mixing with air and, consequently, the  $NO_x$  emissions can reduce. It is the  
 303 contribution of the main combustion that makes the final levels of  $NO_x$  higher for the *pM* injection schedule (cf. Fig.  
 304 13).

305 When the two pilot shots are applied, the *HRR* curve (Fig. 11) remains uninterruptedly higher than zero from the start of  
 306 the cool flames pertaining to the first pilot injection till the end of the main injected fuel combustion. Fig. 14 shows the  
 307 crankshaft angle (*MFB50*) that corresponds to a fuel mass burned fraction equal to  $x_b=0.5$ , and the diagrams plotted in  
 308 Figs. 11 and 14 justify the slight *bsfc* improvement, which in Fig. 8 generally results from the application of the *ppM*  
 309 strategy. In fact, the combustion heat is released closer to the *TDC* in the *ppM* case than in the *pM* one, in part due to the  
 310 more advanced  $SOI_{Main}$ .

311 The fuel for the *ppM* strategy burns with a more regular combustion rate, as can be seen in Fig.11 and without high-time  
 312 derivatives in the burned gas mass fraction time history (cf. also Fig. 14). As a consequence, a remarkable decrease in  
 313 the combustion noise can be expected, and the *CN-NO<sub>x</sub>* curve in Fig. 15 in fact improves significantly for the triple  
 314 injection strategy, compared to the *pM* injection schedule (reductions of up to 3.5 dB can occur). This is a consequence  
 315 of the decrease in the dwell times between the consecutive injection shots, compared to the *pM* case. In fact, the  
 316 reduction in the premixed combustion portion for the *ppM* strategy makes combustion noise decrease. The advanced  
 317  $SOI_{Main}$  in the *ppM* injection pattern was purposely implemented in order to reduce the combustion noise. The mass  
 318 fraction of burned fuel, before the start of the main injection in Fig. 14, is equal to 15% and to 12% for the *pM* and the  
 319 *ppM* strategies, respectively, while the minimum noise condition generally corresponds to approximately 8% [8].

320 Figures 16 and 17 show the combustion noise Fourier spectra, evaluated at  $n=1500$  rpm and  $bmeP=2$  bar, for the *pM* and  
 321 the *ppM* strategies, respectively. The solid bars in each figure refer to the  $X_{EGR} \approx 49 \div 50\%$  case, whereas the hatched bars  
 322 refer to  $X_{EGR} \approx 52 \div 53\%$ . A frequency range ( $500 \div 2000$  Hz), in which the spectral combustion noise takes on the highest  
 323 values, exists in each Fourier spectrum. The presence of a pronounced peak zone, which occurs within a narrow  
 324 frequency band, is more evident for the *pM* diagram at  $X_{EGR} \approx 49 \div 50\%$ , even though the peak zone tends to disappear as  
 325 the value of  $X_{EGR}$  is increased. The presence of a peak zone in the diagrams in Figs. 16 and 17 indicates that there is an  
 326 overly dominant frequency range in the signal, which gives tonality to the noise. In other words, the higher the peak

intensity and the smaller the extension of the peak zone, the more recognizable the combustion noise as a specific noise. The sensitivity of the combustion noise to *EGR* variations is limited for the *ppM* strategy, while the tonality is more reduced for the *pM* pattern as the *EGR* passes from  $X_{EGR} \approx 50\%$  to  $X_{EGR} \approx 53\%$ . Since the human ear is very sensitive to changes in noise, a triple injection can contribute to a less irritating perception of the combustion noise when the *EGR* rate is modified.

Finally, the increase in soot emissions, which can be observable in Figs. 18 and 19 for the triple injection, is not of real concern since the smoke emissions continue to show relatively low values (Soot < 0.31 g/kWh in Fig. 18 and Soot < 0.01 mg in Fig. 19), due to the low peak in-cylinder temperatures and the high relative air-to-fuel ratio ( $\lambda$ ) for these engine working conditions. The presence of a soot- $NO_x$  trade-off curve, in the case of the *ppM* injection strategy, shows that the combustion does not feature *PCCI*-like behavior, unlike the *pM* case.

All of the previous explanations and conclusions about the effects that the addition of a second pilot injection has on engine emissions, combustion noise and *bsfc* performance have been based on experimental data at  $n=1500$  rpm and  $bme_p=2$  bar, but they can be extended to the whole area for light loads, from low to medium engine speeds. This can be confirmed from the experimental results plotted in Figs. 20-24, which refer to  $n=2000$  rpm and  $bme_p=2$  bar. In particular, the double-pilot injection strategy offers the best potentiality to reduce *CN*, *HC* and *CO* with limited penalties on soot emissions. The *ppM* strategy can also lead to an improvement in the startability of a cold engine, which is a typical problem for low-compression ratio engines. In fact, the longer ignition delay and poorer vaporization of the fuel can inhibit fuel ignition, but double-pilot injections are able to contrast this tendency.

## 5. MEDIUM-LOAD CONDITIONS.

Figures 25 and 26 report the *HRR* and  $x_b$  time histories, calculated at  $bme_p=5$  bar and  $n=2000$  rpm for the calibration baseline points of the *pM* and *ppM* strategies, respectively. The *pM* strategy in Fig. 25 does not feature any cool flames because the in-cylinder pressure and the temperature values at the pilot injection timing are more elevated than in the  $bme_p=2$  bar and  $n=1500$  rpm case. Instead, cool flames are present in the *HRR* diagram pertaining to the *ppM* strategy, due to the early injection timing of the pilot 2 shot. The pilot combustion in the *pM* strategy (cf. the solid line with triangle symbols close to  $\theta \approx 355^\circ$  CA in Fig. 25) is more vigorous than in the *ppM* strategy (cf. the solid line with circle symbols close to  $\theta \approx 358^\circ$  CA in Fig. 25), due to the presence, in the former case, of a clear single-stage ignition. On the other hand, since the single-stage ignition delay of the main injected fuel is longer in the *ppM* strategy, the premixed combustion peak at  $\theta \approx 373^\circ$  CA is higher than in the *pM* case. An appreciable mixing-controlled phase is also present at the end of combustion in both the *pM* and the *ppM* strategies.

Figures 27 and 28 show that the  $bsfc$  and  $CN$  have almost the same levels at  $bme_p = 5$  bar and  $n = 2000$  rpm for the two strategies.  $HC$  (Fig. 29) and  $CO$  (Fig. 30) become worse for  $ppM$ , mainly due to the longer autoignition delay, but it should be pointed out that these emissions are not a reason for concern at the considered engine working condition. Figure 31 shows that the  $NO_x$ - $X_{EGR}$  dependence is the same for the two strategies. An appreciable improvement in the  $NO_x$  emissions can be observed in Fig. 32 (these data have been obtained from the three-zone model) for the baseline calibration point when passing from the  $pM$  strategy to the  $ppM$  one. The differences in the  $NO_x$  emissions between the two calibration baseline points could be the result of the different  $\phi$  distributions in the combustion zone, because the peak  $T_b$  values and the residence times at higher temperatures than 1900 K are similar for the two calibrations (cf. Fig. 33). Furthermore, the higher premixing degree of the pilot injected fuel for the  $pM$  injection case makes the  $NO_x$  emissions increase significantly in the  $350^\circ CA \leq \theta \leq 370^\circ CA$  range, compared to the  $ppM$  strategy. A slight deterioration in the soot- $NO_x$   $EGR$  trade-off can be observed in Fig. 34 for the  $ppM$  calibration, even though the maximum soot values in Figs. 34 are not critical, when a diesel particulate filter is mounted. In general, the increased soot emissions represent a penalty for the considered  $ppM$  strategy for medium load and speed conditions (the soot values in Fig. 34 are much higher than in Fig. 18). Any diminution in the ignition delay, for conventional diesel combustion, causes an increase in soot emissions, and the addition of the pilot 1 injection contributes to the reduction of the fuel ignition delay [4]. The liquid fuel injected during the pilot 1 shot and during most of the main injection burns in the presence of combustion flames for the  $ppM$  strategy, and this interference between the liquid jet and the fire is a remarkable source of soot (cf. Fig. 35), which cannot be balanced by the soot oxidation that occurs during the expansion stroke, owing to the high temperatures induced by the retarded combustion (cf. Fig. 36). From this point of view, the oxidation capability of the soot reduces in the  $ppM$  case, during the first part of the expansion stroke, since  $T_b$  is slightly lower than in the  $pM$  case (Figs. 33), but increases in the exhaust manifold, because  $T_{exh}$  is significantly higher in the  $ppM$  strategy (Fig. 36), due to the significant diffusive combustion shown in Fig. 25.

## 6. CONCLUSIONS.

Pilot-pilot-main injection strategies have been compared with pilot-main injection strategies in a low-compression ratio Euro 5 diesel engine in order to evaluate the possible benefits in engine-out emissions, combustion noise and fuel consumption. The considered pilot-main injection represents the state-of-the art double injection strategy for the considered engine technology, whereas the parameters of the triple injection strategies have been optimized by means of a *DoE* procedure. This innovative approach has allowed an effective assessment of the double pilot injection strategy in partial *PCCI*-like engine working conditions to be made, since optimized double- and triple-injection engine calibrations have been

386 compared. *EGR* trade-offs have been performed in the neighborhood of the baseline points that refer to both the original  
387 double-injection calibration and the triple-injection calibration optimized with the *DoE*.

388 The research investigation has been performed on the basis of experimental tests that were conducted on the engine,  
389 fueled with conventional diesel fuel, in a dynamometer cell. The tests have been carried out at different steady-state  
390 key-points that are representative of engine application in a vehicle over the new European driving cycle for passenger  
391 cars. The experimental analysis has been supported by numerical results that were derived from the application of  
392 diagnostic combustion models to the in-cylinder pressure time history. The main conclusions of the present work are  
393 outlined in a synoptic way as follows.

394 • The application of *EGR* rates close to 50% and of retarded main injection timings allows the  $NO_x$  and the soot  
395 emissions to be decreased simultaneously in late *PCCI* double-injection strategies, due to an intensified fuel premixing  
396 and to a reduced peak combustion temperature. The main drawbacks of these strategies at low loads are the elevated  
397 combustion noise, which is due to the highly premixed combustion, and the high *HC* and *CO* engine-out emissions. The  
398 high *HC* levels at the engine exhaust are generated because of the presence of overmixing regions and wall quenching  
399 phenomena, whereas the high *CO* engine-out emissions are produced by the relatively low in-cylinder temperature and  
400 long fuel ignition delay. Furthermore, the engine *bsfc* deteriorates, compared to the double injection strategies  
401 implemented in conventional diesel engines, due to the retarded main injection timing and the reduced engine  
402 compression ratio.

403 • The employment of pilot-pilot-main injection strategies at light loads and low speeds induces an increase in the  
404 time-averaged value of  $p_{cyl}$ , compared to the *pM* injection schedule, but the *HHR* combustion peaks reduce, due to the  
405 fuel ignition delay diminution. The *ppM* pattern, when applied to a late *PCCI* injection strategy, leads to an increase in  
406 the local fuel concentration, with respect to time and space. The generation of a suitable fuel vapor stratification, close  
407 to the nozzle, reduces the impact of fuel overmixing and wall quenching and thus decreases the *HC* and *CO* engine-out  
408 emissions. Significant reductions in the combustion noise, of up to 4dB, can be obtained, compared to the double  
409 injection schedule. The changes in the *CN* tonality, as the *EGR* rate varies, are more pronounced for the *pM* strategy  
410 than for the *ppM* one and this leads, in the latter case, to a less irritating perception of the combustion noise when the  
411 *EGR* rate is modified. Finally, slight improvements in the *bsfc-NO<sub>x</sub>* *EGR* trade-off can be observed for the case of the  
412 *ppM* injection schedule.

413 • At medium engine loads and speeds, the late *PCCI* pilot-pilot-main strategy optimized with the *DoE* allows the  
414  $NO_x$  engine-out emissions to be decreased significantly, compared to the baseline point of the *pM* injection calibration.  
415 However, the  $NO_x$ -soot trade-off curve of the *pM* strategy is not improved and soot penalties are therefore incurred for  
416 the *ppM* baseline calibration point, even though they are acceptable when a diesel particulate filter is mounted. The *CN*-

417  $NO_x$ , the  $bsfc$ -  $NO_x$ , the  $HC$ -  $NO_x$  and the  $CO$ - $NO_x$   $EGR$  curves do not change appreciably when the second pilot shot is  
418 added to the  $ppM$  injection train.

419 • On the basis of the results of the present work, a  $ppM$  injection strategy is recommended for low loads and speeds  
420 to improve engine-out emissions and noise in low compression ratio engines characterized by high  $EGR$  rates. On the  
421 other hand,  $ppM$  strategies do not seem to lead to any significant benefits in the higher part of the  $NEDC$ , compared to  
422 optimized  $ppM$  strategies, for the considered engine typology. Nevertheless, the choice of the most efficient calibration  
423 for an engine depends to a great extent on the coupling of the combustion system to the aftertreatment devices that are  
424 installed on the engine. Therefore, the  $ppM$  strategy could be considered for medium load and engine speeds in order to  
425 minimize  $NO_x$  emissions.

## 426 7. NOMENCLATURE.

427	$bmeP$	brake mean effective pressure
428	$bsfc$	brake specific fuel consumption
429	$CA$	crank angle degree
430	$CN$	combustion noise
431	$DT_1$	dwel time between the pilot 1 and main injection shots
432	$DT_l$	dwel time between the pilot 2 and pilot 1 injection shots
433	$ECU$	electronic control unit
434	$EGR$	exhaust gas recirculation
435	$HC$	unburned hydrocarbons
436	$HRR$	heat release rate
437	$m_a$	inducted air per engine cycle and per cylinder
438	$\dot{m}_a$	fresh air mass flow-rate
439	$\dot{m}_{EGR}$	exhaust gas mass flow-rate
440	$MFB50$	angle at which 50% of the combustion mixture has burned
441	$n$	engine speed
442	$NO_x$	nitrogen oxides
443	$OEM$	original equipment manufacturer
444	$p_{cyl}$	in-cylinder pressure
445	$p_{rail}$	nominal rail pressure level
446	$PCCI$	premixed charge compression ignition



447	$PM$	particulate matter
448	$q_{Pil1}$	volume of fuel injected in the pilot 1 injection
449	$q_{Pil2}$	volume of fuel injected in the pilot 2 injection
450	$SOI_{Main}$	electrical start of the main injection
451	$SOI_{Pil}$	electrical start of the pilot injection
452	$Sw$	swirl actuator position
453	$T_b$	burned gas temperature
454	$TDC$	top dead center
455	$X_{EGR}$	mass fraction of exhaust gas recirculation
456	$\phi$	equivalence ratio
457	$\lambda$	relative air-to-fuel ratio
458	$\theta$	crankshaft angle in the simulations

## 459    **8. REFERENCES.**

- 460    [1] Heywood, J. B., 1988, “Internal combustion engine fundamentals”, McGraw Hill, New York.
- 461    [2] Maiboom, A., Tauzia, X., and Hetet, J. F., 2008, “Experimental study of various effects of exhaust gas  
462    recirculation on combustion and emissions of an automotive direct injection diesel engine”, *Energy*, 33,  
463    pp. 22-34.
- 464    [3] Ehleskog, R., Ochoterena, R. L., and Andersson, S., 2007, “Effects of multiple injections on engine-out  
465    emission levels including particulate mass from an HSDI diesel engine”, SAE paper. 2007-01-0910.
- 466    [4] Suh, K. H., 2014, “Study on the twin-pilot-injection strategies for the reduction in the exhaust emissions  
467    in a ow-compression engine”, *Proc. IMechE Part D: J. of Automobile Engineering*, vol. 228(3), pp. 335-343.
- 468    [5] Lee, J. W., Choi, S. M., Yu, S., Choi, H., and Min, K. D., 2013, “Comparison of the effects of multiple  
469    injection strategy on the emissions between moderate and heavy EGR rate conditions: part 1-pilot  
470    injections”, *Journal of Mechanical Science and Technology*, 27(4), pp. 1135-1141.
- 471    [6] Tullis, S., and Greeves, G., 1996, “ Improving  $NO_x$  versus bsfc with EUI 200 using EGR and pilot  
472    injection for heavy duty diesel engines”, SAE paper No. 960843.

- 473 [7] Bhatt, N. M., Rathod, P. P., Sorathiya, A. S., and Patel, R., 2013, "Effect of the multiple injection on the  
474 performance and emission of diesel engine. A review study", *International Journal of Emerging Technology  
475 and Advanced Technology*, vol. 3 (3).
- 476 [8] Busch, S., Zha, K. and Miles, P.C., 2014, "Investigations of closely coupled pilot and main injections as a  
477 mean to reduce combustion noise", 8<sup>th</sup> Thiesel Conference, Valencia 9<sup>th</sup>-12<sup>th</sup> September.
- 478 [9] Han, Z., Uludogan, A., Hampson, G. J., and Reitz, R. D., 1996, "Mechanism of soot and NO<sub>x</sub> emission  
479 reduction using multiple-injection in diesel engine", SAE paper 960633.
- 480 [10] Yun, H. H., Sellnau, M., Milovanovic, N., and Zuelch, S., 2008, "Development of premixed low-  
481 temperature diesel combustion in a HSDI engine", SAE paper no. 2008-01-0639.
- 482 [11] Helmantel, A., and Golovitchev, 2009, "Injection strategy optimization for a light duty DI diesel engine  
483 in medium load conditions with high EGR rates", SAE paper no. 2009-01-1441.
- 484 [12] Nishimura, T., Satoh, K., Takahashi, S., and Yokota, K., 1998, "Effects of fuel injection rate on  
485 combustion and emission in a DI diesel engine", SAE paper 981929.
- 486 [13] DieselNet, Engine and emission technology online, since 1997, [www.dieselnets.com](http://www.dieselnets.com).
- 487 [14] Kastner, O., Atzler, F., Juvenelle, C., Rotondi, R., and Weigand, A., 2009, "Directly actuated piezo  
488 injector for advanced injection strategies towards cleaner diesel engines" Towards Clean Diesel Engines,  
489 TCDE 2009.
- 490 [15] Predelli, O., Gratzke, R., Sommer, A., Marohn, R., Atzler, F., Schule, H., Kastner, O., and Nozeran, N.,  
491 2010, "Continuous injection-rate shaping for passenger-car diesel engines – Potential, limits and feasibility",  
492 31<sup>st</sup> International Vienna Engine Symposium.
- 493 [16] Payri, F., Broatch, A., Salavert, J. M., Martín, J.,  
494 2010, "Investigation of Diesel combustion using multiple injection strategies for idling after cold start of  
495 passenger-car engines", *Experimental Thermal and Fluid Science*, 34, pp. 857–865.
- 496 [17] Tow, T. C., Pierpont, D. A., and Reitz, R. D., 1994, "Reducing Particulate and NO<sub>x</sub> emissions by using  
497 multiple injections in a heavy duty D.I. diesel engine", SAE paper 940897.

498 [18] Hotta, Y., Inayoshi, M., Nakakita, K., Fujiwara, K., and Sakata, I., 2005, “ Achieving lower exhaust  
 499 emissions and better performance in an HSDI diesel engine with multiple injection”, SAE paper no. 2005-  
 500 01-0928.

501 [19] Badami, M., Mallamo, F., Millo, F., and Rossi, E. E., 2003, “Experimental investigation on the effect of  
 502 multiple injection strategies on emissions, noise and brake specific fuel consumption of an automotive direct  
 503 injection common-rail diesel engine”, *International journal of engine research* 4(4), pp. 299-314.

504 [20] Okude, K., Mori, K., Shiino, S., Yamada, K., and Matsumoto, Y., 2007, “Effects of multiple injections  
 505 on diesel emission and combustion characteristics”, SAE paper. No. 2007-01-4178.

506 [21] Mobasheri, R. Peng, Z., 2012, “Investigation of pilot and multiple injection parameters on mixture  
 507 formation and combustion characteristics in a heavy duty DI-diesel engine”, SAE paper 2012-04-16.

508 [22] Schoppe, D., Zulch, S., Harfy, M., Geurts, D., Jaorach, R. W., and Baker, N., ,2008, “Delphi Common  
 509 rail system with direct acting injector”, MTZ 10/2008, vol. 69, pp. 32-38.

510 [23] Ricaud, J.C., and Lavoisier, F., 2004, “Optimizing the multipleinjection settings on an HSDI diesel  
 511 engine” Conference on Thermo- and fluid-dynamics processes in diesel Engines, Valencia, Spain, 11–13  
 512 September 2002

513 [24] Zheng Z, Yue L, Liu H, Zhu Y, Zhong X, Yao M, 2015, “Effect of two-stage injection on combustion  
 514 and emissions under high EGR rate on a diesel engine by fueling blends of diesel/gasoline, diesel/n-butanol,  
 515 diesel/gasoline/n-butanol and pure diesel”, *Energy Conversion and Management*, 90, pp. 1-15.

516 [25] d'Ambrosio, S., Finesso, R., and Spessa, E., 2011, “Calculation of Mass Emissions, Oxygen Mass  
 517 Fraction And Thermal Capacity Of The Inducted Charge In SI And Diesel Engines From Exhaust And  
 518 Intake Gas Analysis”, *Fuel*, n. 90, issue 1, pp. 152-166.

519 [26] Finesso, R., and Spessa, E, 2014, “A real time zero-dimensional diagnostic model for the calculation of  
 520 in-cylinder temperatures, HRR and nitrogen oxides in diesel engines. *Energy Conversion and Management*  
 521 79 498–510. <http://dx.doi.org/10.1016/j.enconman.2013.12.045>.

- 522 [27] Baratta M., Catania A.E., Ferrari A., Finesso R. and Spessa E., 2011, “Premixed-Diffusive Multizone  
523 Model for Combustion Diagnostics in Conventional and PCCI Diesel Engines”, *ASME Trans. Journal of*  
524 *Engineering for Gas Turbines and Power*, vol. 133 n. 10, Art. No. 102801, pp. 1-13.
- 525 [28] Fang C, Yang F, Ouyang M, Gao G, Chen L, 2013, “Combustion mode switching control in a HCCI  
526 diesel engine, *Applied Energy* 110 (2013) 190–200”, <http://dx.doi.org/10.1016/j.apenergy.2013.04.060>.
- 527 [29] Agarwal D, Singh SK, Agarwal AK, 2011, “Effect of exhaust gas recirculation (EGR) on performance,  
528 emissions, deposits and durability of a constant speed compression ignition engine”. *Applied Energy*  
529 2011;88(8):2900–7.
- 530 [30] Kiplimo, R., Tomita, E., Kawahara, N., and Yokobe, S., 2012, “Effects of spray impingement, injection  
531 parameters and EGR on the combustion and emission characteristics of a PCCI diesel engine”, *Applied*  
532 *Thermal Engineering*, vol. 37, pp. 165-175.
- 533 [31] Mendez, S., and Thirouard, B., 2008, “Using multiple injection strategies in diesel combustion: potential  
534 to improve emissions, noise and fuel economy trade-off in low CR engine”, SAE paper 2008-01-1329.
- 535 [32] Broath, A., Ruiz, S., Margot, X., and Gil, A., 2010, “Methodology to estimate the threshold in-cylinder  
536 temperature for self-ignition of fuel during cold start of diesel engines”, *Energy*, 35, pp. 2251-2560
- 537 [33] McMillan, D., La Rocca, A., Shayler, P. J., et al., 2008, “The effect of reducing compression ratio on  
538 the work output and heat release characteristics of a DI diesel under cold start conditions”, SAE Paper No.  
539 2008-01-1306.
- 540 [34] Kiplimo R, Tomita, Kawahara N, Yokobe S, 2012, “Effects of spray impingement, injection parameters,  
541 and EGR on the combustion and emission characteristics of a PCCI diesel engine”, *Applied Thermal*  
542 *Engineering* 37 (2012) 165-175. doi:10.1016/j.applthermaleng.2011.11.011.
- 543 [35] Saxena S, Dedoya ID, 2013, “Fundamental phenomena affecting low temperature combustion and  
544 HCCI engines, high load limits and strategies for extending these limits, *Progress in Energy and Combustion*  
545 *Science* 39 (2013) 457-488. <http://dx.doi.org/10.1016/j.pecs.2013.05.002>.

[36] Suh HK, Investigations of multiple injection strategies for the improvement of combustion and exhaust emissions characteristics in a low compression ratio (CR) engine, 2011, *Applied Energy* 88 (2011) 5013–5019. doi:10.1016/j.apenergy.2011.06.048.

[37] Dec, J., and Canaan, R. E., 1998 “PLIF imaging of NO formation in a DI diesel engine”, *SAE Transactions*, 107, No. 3, pp. 176-204.

[38] Akihama, K., Takatori, Y., Inagaki, K., Sakaki, S., and Dean, A. M., 2001, “Mechanism of smokeless rich diesel combustion by reducing temperature”, SAE paper no. 2001-01-0655.

9. TABLES AND FIGURES

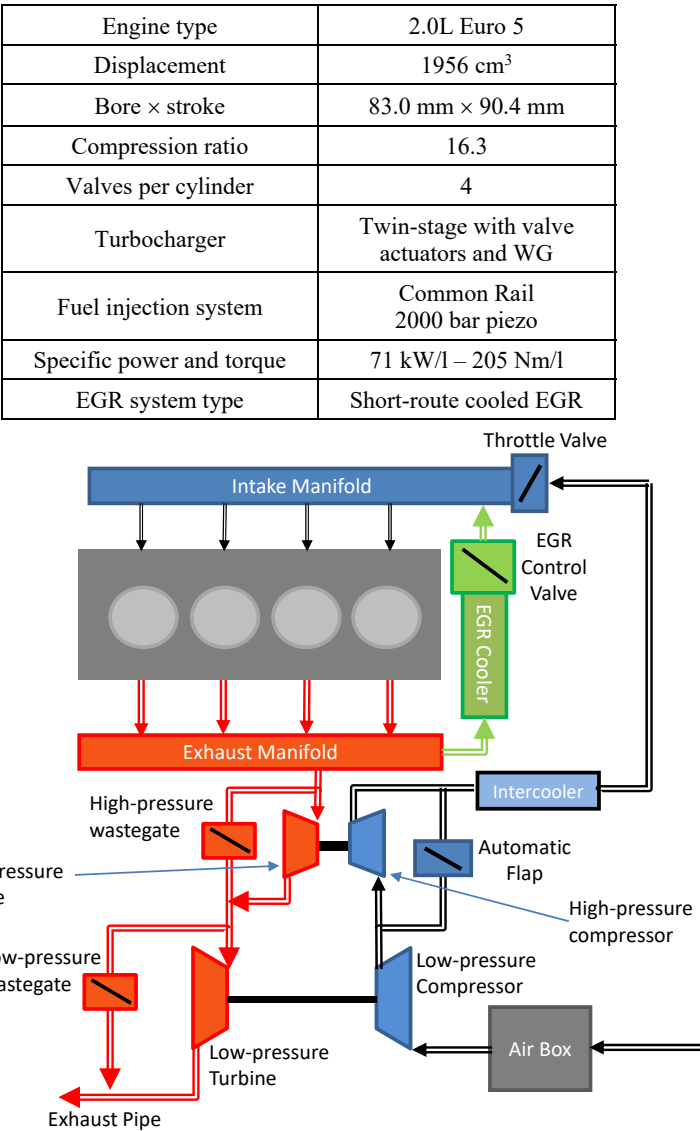


Table 1. Main specifications and schematic of the tested engine.

Quantity	Levels	Optimization
$SOI_{Main}$ [°CA bTDC]	-4.5 -2.88 -1.25 0.37 2	-0.2
$m_a$ [mm <sup>3</sup> /(stk·cyl)]	230 245 260	230
$S_w$ [%]	30 38.8 47.5 56.3 65	39.7
$p_{Rail}$ [bar]	300 450 600	516.6
$q_{Pil1}$ [mm <sup>3</sup> /(stk·cyl)]	0.8 1.23 1.65 2.08 2.5	1
$DT_1$ [μs]	300 625 950 1275 1600	446
$q_{Pil2}$ [mm <sup>3</sup> /(stk·cyl)]	0.8 1.1 1.4 1.7 2	2
$DT_2$ [μs]	300 625 950 1275 1600	907

**Table 2: Levels considered in the variation list and optimized values of the input variables for the triple injection at 1500×2.**

555

556

Quantity	Levels	Optimization
$SOI_{Main}$ [°CA bTDC]	-1 1 3	1
$m_a$ [mm <sup>3</sup> /(stk·cyl)]	360 380 390 400 420	362.2
$S_w$ [%]	30 38.8 47.5 56.3 65	35.5
$p_{Rail}$ [bar]	750 833.3 950 1016.7 1150	826.4
$q_{Pill}$ [mm <sup>3</sup> /(stk·cyl)]	0.8 1.23 1.65 2.08 2.5	0.8
$DT_1$ [μs]	300 625 950 1275 1600	773
$q_{Pill}$ [mm <sup>3</sup> /(stk·cyl)]	0.8 1.1 1.4 1.7 2	0.8
$DT_2$ [μs]	600 850 1100 1350 1600	1600

**Table 3: Levels considered in the variation list and optimized values of the input variables for the triple injection at 2000×5.**

Strategy	NO <sub>x</sub> [g/kWh]	HC [g/kWh]	CO [g/kWh]	Soot [g/kWh]	bsfc [g/kWh]	CN [dBA]
pM	0.53	2	8.8	0.04	299	76.7
ppM	min	≤2	≤9	≤0.3	≤305	≤74

**Table 4: Reference values of the reference *pM* calibration baseline point and constraints for the optimization of the *ppM* injection strategy at 1500×2.**



Strategy	NO <sub>x</sub> [g/kWh]	HC [g/kWh]	CO [g/kWh]	Soot [g/kWh]	bsfc [g/kWh]	CN [dBA]
pM	0.99	0.3	1.9	0.3	248	86.5
ppM	min	≤0.5	≤5	≤1.2	≤255	≤86.5

**Table 5.** Reference values of the reference *pM* calibration baseline point and constraints for the optimization of the *ppM* injection strategy at 2000×5.

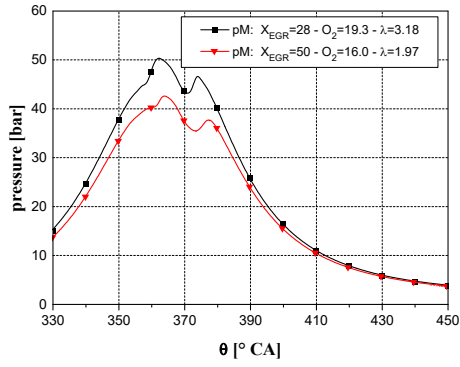


Figure 1.  $p_{cyl}$  versus  $\theta$  distribution for  $X_{EGR}=28\%$  and  $X_{EGR}=50\%$  ( $bmep=2$  bar,  $n=1500$  rpm).

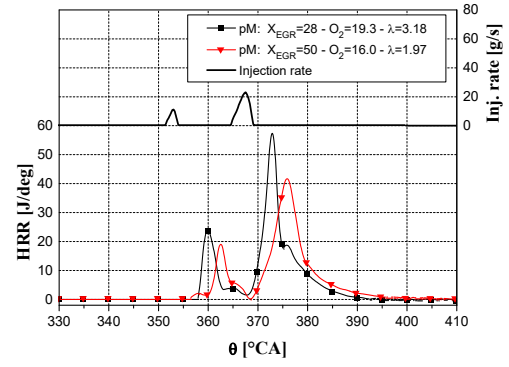


Figure 2. HRR versus  $\theta$  distribution for  $X_{EGR}=28\%$  and  $X_{EGR}=50\%$  ( $bmep=2$  bar,  $n=1500$  rpm).

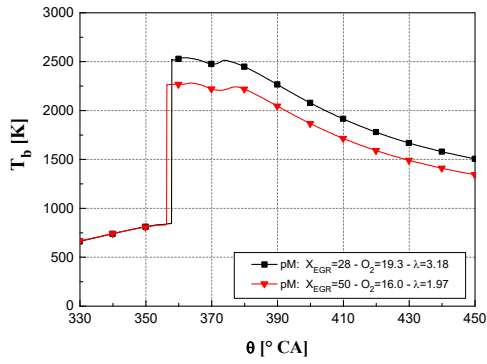


Figure 3.  $T_b$  versus  $\theta$  distribution for  $X_{EGR}=28\%$  and  $X_{EGR}=50\%$  ( $bmep=2$  bar,  $n=1500$  rpm).

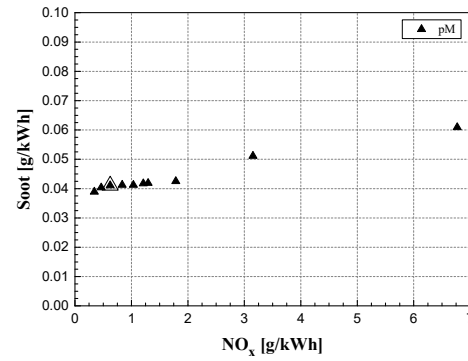


Figure 4. Soot-  $NO_x$  for different  $X_{EGR}$  values ( $bmep=2$  bar,  $n=1500$  rpm).

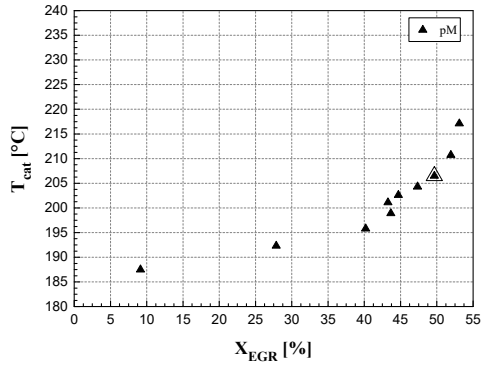


Figure 5. Gas temperature  $T_{cat}$  as a function of  $X_{EGR}$  ( $bmep=2$  bar,  $n=1500$  rpm).

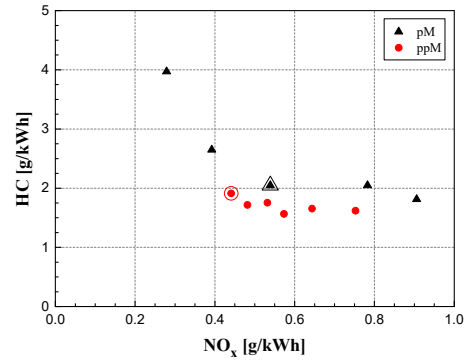


Figure 6. HC- $NO_x$  trade-off for the pM and ppM strategies ( $bmep=2$  bar,  $n=1500$  rpm).

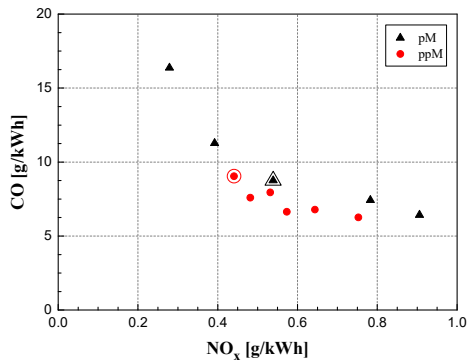


Figure 7. CO- $NO_x$  trade-off for the pM and ppM strategies ( $bmep=2$  bar,  $n=1500$  rpm).

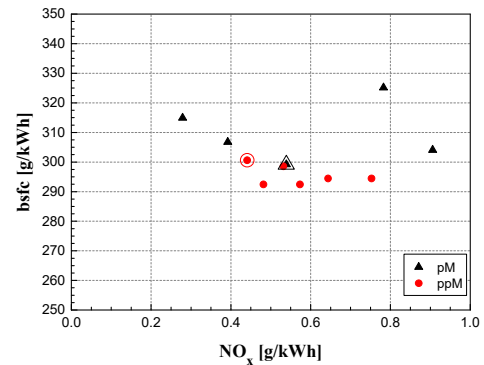


Figure 8. bsfc- $NO_x$  trade-off for the pM and ppM strategies ( $bmep=2$  bar,  $n=1500$  rpm).

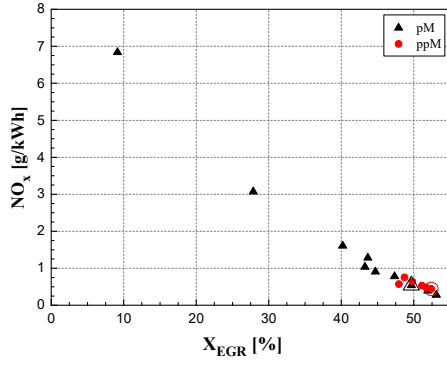


Figure 9.  $NO_x$  versus  $X_{EGR}$  for the  $pM$  and  $ppM$  strategies ( $bmp=2$  bar,  $n=1500$  rpm).

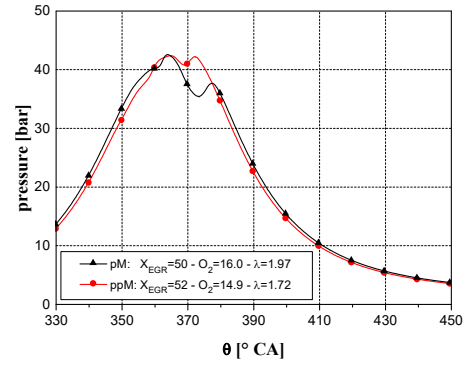


Figure 10.  $p_{cyl}$  versus  $\theta$  distribution for  $pM$  and  $ppM$  strategies ( $bmp=2$  bar,  $n=1500$  rpm).

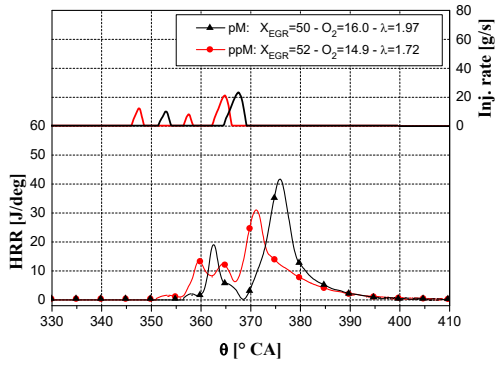


Figure 11. HRR versus  $\theta$  distribution for the  $pM$  and  $ppM$  strategies ( $bmp=2$  bar,  $n=1500$  rpm)

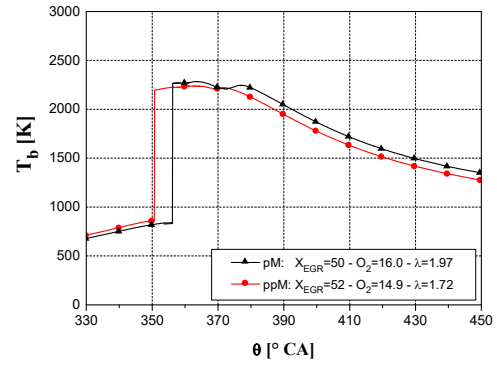


Figure 12.  $T_b$  versus  $\theta$  distribution for  $pM$  and  $ppM$  strategies ( $bmp=2$  bar,  $n=1500$  rpm).

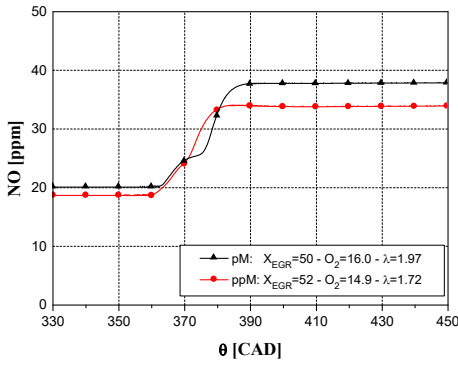


Figure 13.  $NO$  versus  $\theta$  distribution for  $pM$  and  $ppM$  strategies ( $bmp=2$  bar,  $n=1500$  rpm).

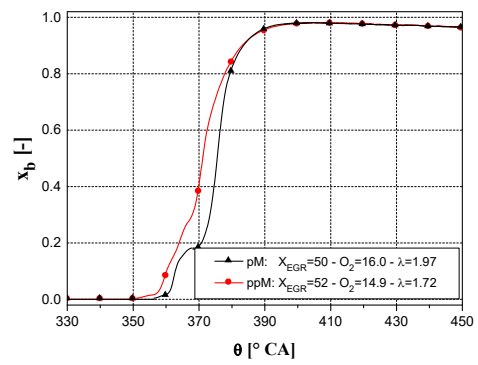


Figure 14.  $x_b$  versus  $\theta$  distribution for  $pM$  and  $ppM$  strategies ( $bmp=2$  bar,  $n=1500$  rpm).

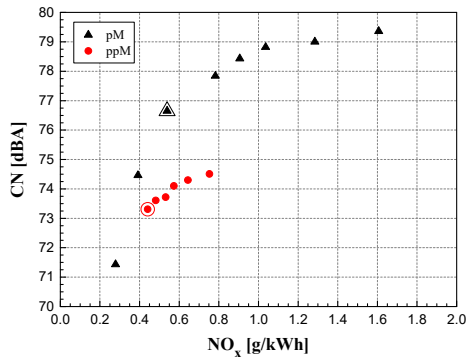


Figure 15.  $CN-NO_x$  trade-off for the  $pM$  and  $ppM$  strategies ( $bmp=2$  bar,  $n=1500$  rpm).

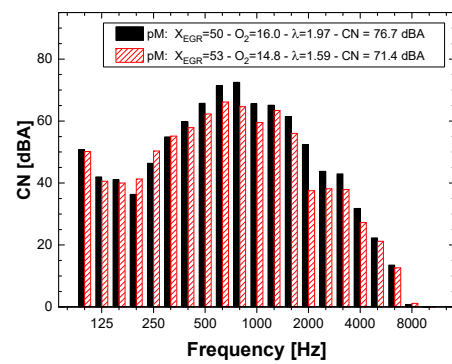


Figure 16. One-third octave frequency bands of  $CN$  for the  $pM$  strategy ( $bmp=2$  bar,  $n=1500$  rpm).

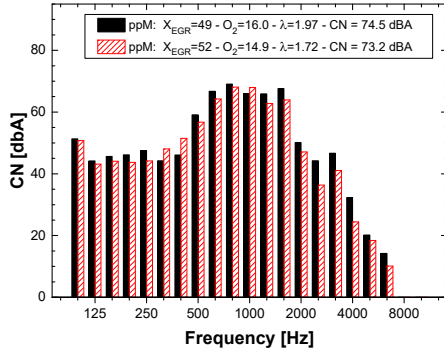


Figure 17. One-third octave frequency bands of  $CN$  for the  $ppM$  strategy ( $bmp=2$  bar,  $n=1500$  rpm).

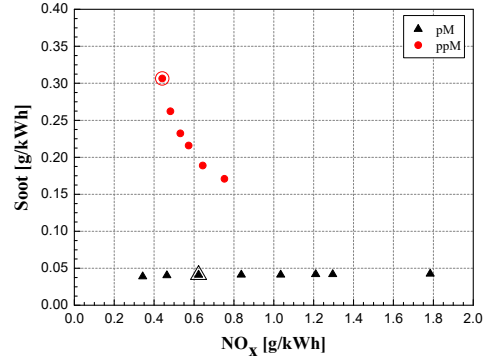


Figure 18. Soot- $NO_x$  trade-off for the  $ppM$  strategy ( $bmp=2$  bar,  $n=1500$  rpm).

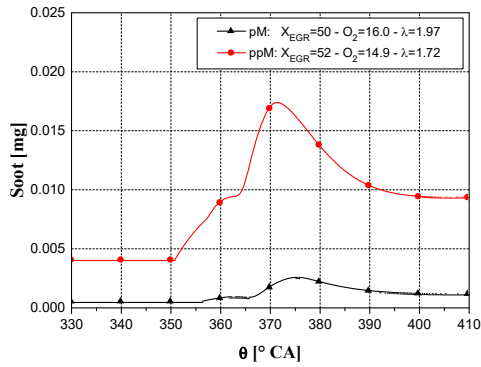


Figure 19.  $PM$  versus  $\theta$  distribution for  $pM$  and  $ppM$  strategies ( $bmp=2$  bar,  $n=1500$  rpm).

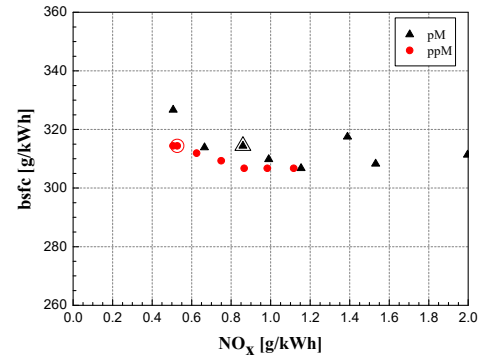


Figure 20.  $bsfc$ - $NO_x$  trade-off for the  $pM$  and  $ppM$  strategies ( $bmp=2$  bar,  $n=2000$  rpm).

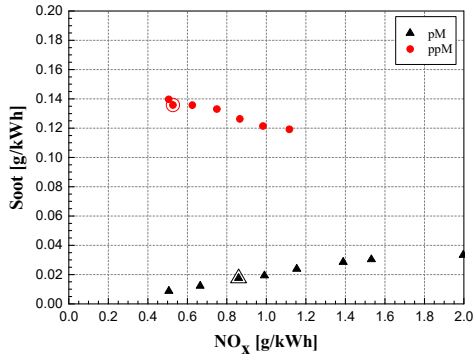


Figure 21. Soot- $NO_x$  trade-off for the  $pM$  and  $ppM$  strategies ( $bmp=2$  bar,  $n=2000$  rpm).

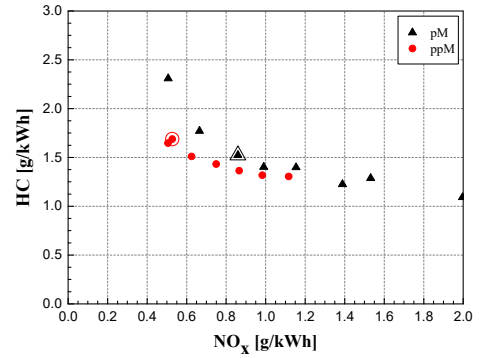


Figure 22.  $HC$ - $NO_x$  trade-off for the  $pM$  and  $ppM$  strategies ( $bmp=2$  bar,  $n=2000$  rpm).

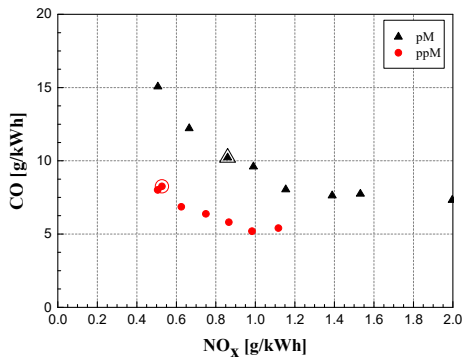


Figure 23.  $CO$ - $NO_x$  trade-off for the  $pM$  and  $ppM$  strategies ( $bmp=2$  bar,  $n=2000$  rpm).

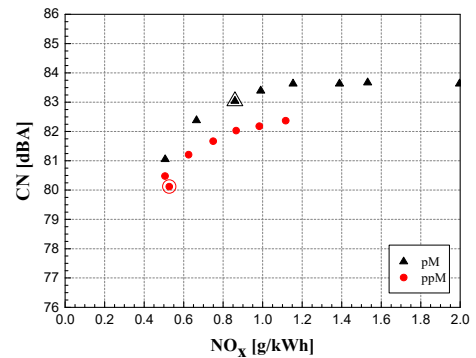


Figure 24.  $CN$ - $NO_x$  trade-off for the  $pM$  and  $ppM$  strategies ( $bmp=2$  bar,  $n=2000$  rpm).

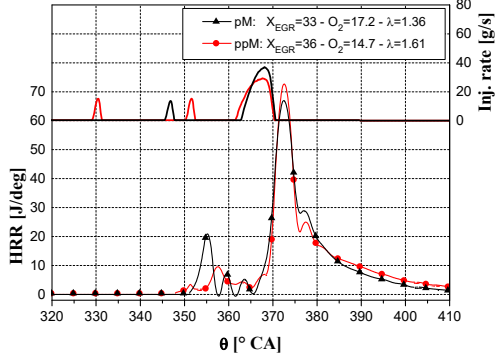


Figure 25. HRR versus  $\theta$  distribution for the *pM* and *ppM* strategies (*bmp*=5 bar, *n*=2000 rpm).

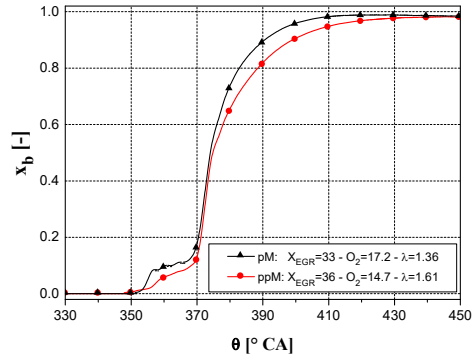


Figure 26.  $x_b$  versus  $\theta$  distribution for *pM* and *ppM* strategies (*bmp*=5 bar, *n*=2000 rpm).

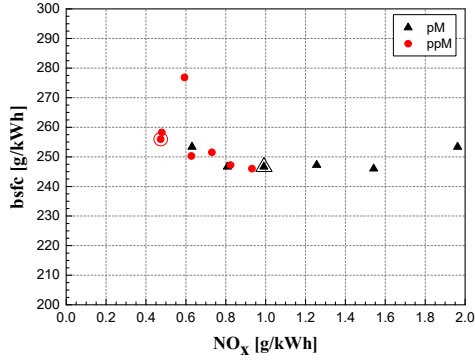


Figure 27. *bsfc*- $NO_x$  trade-off for the *pM* and *ppM* strategies (*bmp*=5 bar, *n*=2000 rpm).

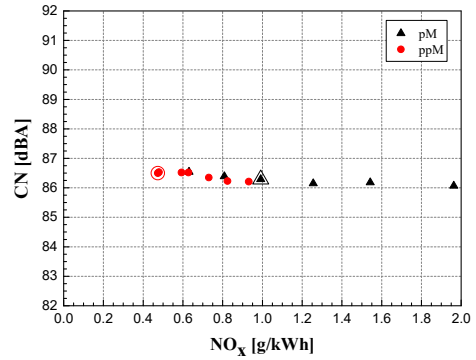


Figure 28. *CN*- $NO_x$  trade-off for the *pM* and *ppM* strategies (*bmp*=5 bar, *n*=2000 rpm).

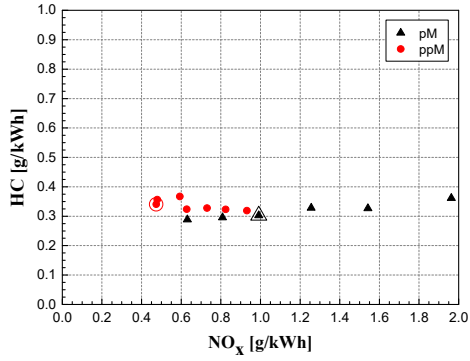


Figure 29. *HC*- $NO_x$  trade-off for the *pM* and *ppM* strategies (*bmp*=5 bar, *n*=2000 rpm).

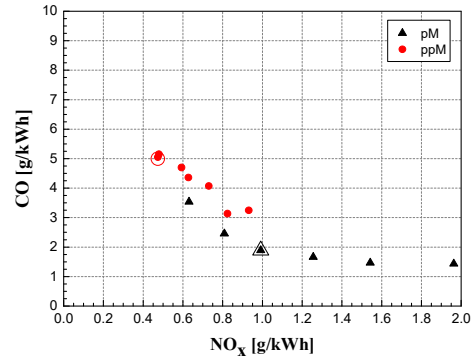


Figure 30. *CO*- $NO_x$  trade-off for the *pM* and *ppM* strategies (*bmp*=5 bar, *n*=2000 rpm).

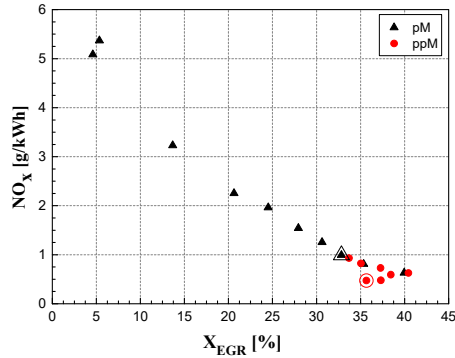


Figure 31.  $NO_x$  versus  $X_{EGR}$  for the *pM* and *ppM* strategies (*bmp*=5 bar, *n*=2000 rpm).

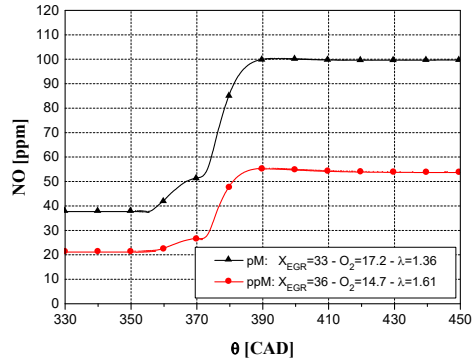


Figure 32.  $NO_x$  versus  $\theta$  distribution for the *pM* and *ppM* strategies (*bmp*=5 bar, *n*=2000 rpm).

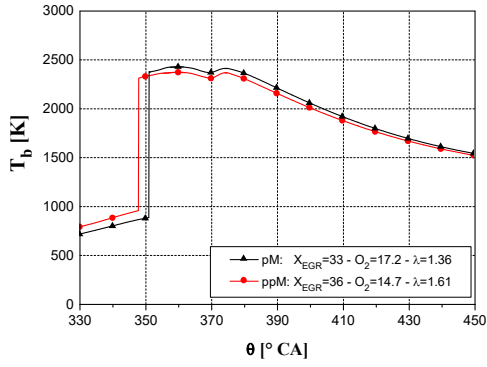


Figure 33.  $T_b$  versus  $\theta$  distribution for  $pM$  and  $ppM$  strategies ( $bmeP=5$  bar,  $n=2000$  rpm).

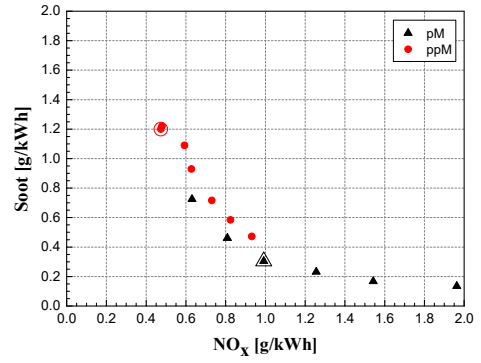


Figure 34. Soot- $NO_x$  trade-off for the  $pM$  and  $ppM$  strategies ( $bmeP=5$  bar,  $n=2000$  rpm).

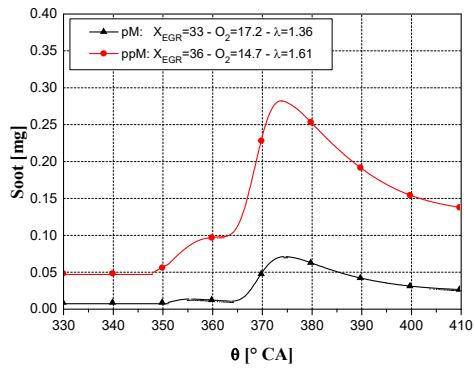


Figure 35. Soot versus  $\theta$  distribution for the  $pM$  and  $ppM$  strategies ( $bmeP=5$  bar,  $n=2000$  rpm).

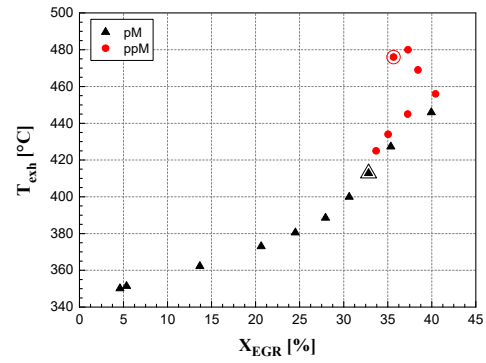


Figure 36.  $T_{exh}$  versus  $X_{EGR}$  for the  $pM$  and  $ppM$  strategies ( $bmeP=5$  bar,  $n=2000$  rpm).